Inorganic Chemistry

ARTICLE

pubs.acs.org/IC

Wet Chemical Synthesis and a Combined X-ray and Mössbauer Study of the Formation of $FeSb_2$ Nanoparticles

Christina S. Birkel,[†] Gregor Kieslich,[†] Dimitrios Bessas,[§,∥] Tania Claudio,[§,∥] Robert Branscheid,[‡] Ute Kolb,[‡] Martin Panthöfer,[†] Raphaël P. Hermann,[*,§,∥] and Wolfgang Tremel[*,†]

[†]Institut für Anorganische Chemie und Analytische Chemie, Johannes Gutenberg-Universität, Duesbergweg 10-14, D-55099 Mainz, Germany

[‡]Institut für Physikalische Chemie, Johannes Gutenberg-Universität, Welderweg 11, D-55099 Mainz, Germany

[§]Jülich Centre for Neutron Science JCNS and Peter Grünberg Institut PGI, JARA-FIT, Forschungszentrum Jülich GmbH, D-52425 Jülich, Germany

[∥]Faculté des Sciences, Université de Liège, B-4000 Liège, Belgium

Supporting Information

ABSTRACT: Understanding how solids form is a challenging task, and few strategies allow for elucidation of reaction pathways that are useful for designing the synthesis of solids. Here, we report a powerful solution-mediated approach for formation of nanocrystals of the thermoelectrically promising $FeSb_2$ that uses activated metal nanoparticles as precursors. The small particle size of the reactants ensures minimum diffusion paths, low activation barriers, and low reaction temperatures, thereby eliminating solid−solid diffusion as the rate-limiting step in conventional bulk-scale solid-state synthesis. A time- and temperature-dependent study of formation of nanoparticular $FeSb_2$ by X-ray powder diffraction and iron-57 Mössbauer spectroscopy showed the incipient formation of the binary phase in the temperature range of 200−250 °C.

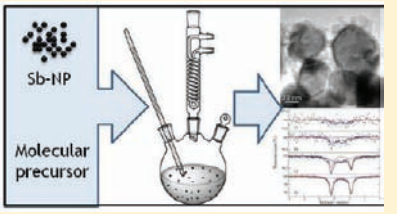

INTRODUCTION

Intermetallic compounds are among the most prominent materials in industry because their crystalline order gives rise to superior physical properties in comparison to less-ordered alloys.[1] Additionally, reducing the particle size allows further changes and adjustment of the nanoparticle properties as opposed to their bulk behavior.[2]

Within the antimonide group of compounds researchers can find materials with a wide variety of possible applications, for example, as battery anode materials[3,4] and in superconducting[5−8] and thermoelectric devices.[9−15] These properties make them useful compounds from an industrial point of view as well as important and interesting systems to study from an academic point of view.

With regard to its thermoelectric properties, $FeSb_2$ has been shown to exhibit a colossal Seebeck coefficient at temperatures of around 10 K. This colossal Seebeck coefficient was related to the electronic structure of the strongly correlated $FeSb_2$ semiconductor. The drawback of $FeSb_2$ is its relatively high thermal conductivity which reduces its overall thermoelectric performance significantly.[16−18] The findings of Dresselhaus and Hicks in the early 1990s[19,20] sparked numerous studies of nanoparticular systems. In recent years, several groups have successfully reported improved performances for nanostructured materials.[21−26] To further contribute to this field of research, synthetic routes toward nanostructured antimonides need to be explored and optimized.

Synthesis of intermetallic compounds usually requires high reaction temperatures as well as long reaction times. Possible synthetic routes include arc melting in an inert atmosphere,[27] heating for an extended period of time in a fused silica ampule,[28] or flux growth techniques.[29−31] Due to the intrinsically metastable state of nanosized materials such reaction conditions are not practicable. Therefore, the number of low-temperature synthetic approaches to nanocrystalline intermetallic compounds has increased over the past few years. Elegant synthetic strategies based on in situ reduction in high-boiling solvents, (modified) polyol processes,[32,33] and solvothermal reactions allow the synthesis of binary and ternary as well as metastable intermetallic phases.[34,35] However, while top-down approaches such as ball milling have been used to fabricate antimonide nanoparticles,[36−38] the bottom-up synthesis of these materials has not been focused on intensively.

Using a wet chemical approach, it could be demonstrated that nanoparticular zinc antimonide is formed at temperatures below 300 °C through reaction of activated metal nanoparticles.[39] Inspired by this work, we recently extended that approach to a solution-based synthetic route in which Sb and Zn nanoparticles subsequently react in trioctylamine to form a binary antimonide phase. Through these particular experimental conditions a new Zn−Sb compound ($Zn_{1+\delta}Sb$) was identified, and its structure

Received: September 4, 2011
Published: October 17, 2011

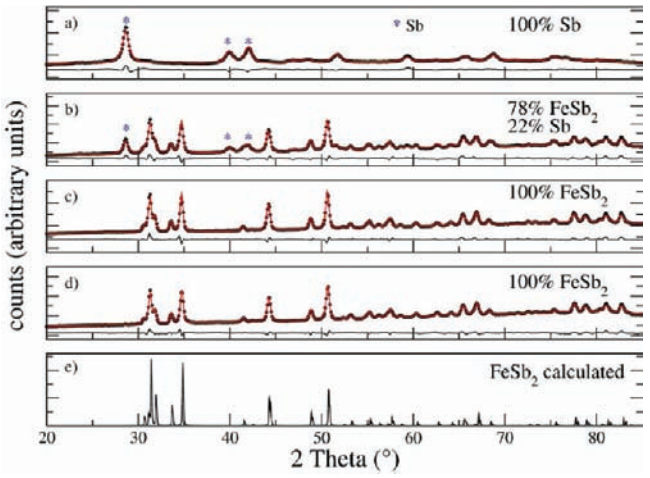

Figure 1. Time-dependent (ex situ) X-ray diffraction (experimental data, black circles), Rietveld fits (red line), and corresponding difference plots (black line) at different reaction temperatures and times. Data from samples taken at (a) ~200 °C, (b) ~250 °C, (c) ~300 °C, and (d) ~300 °C after 60 min; (e) calculated diffractogram of $FeSb_2$.

was determined by electron diffraction tomography.[35] The flexibility and potential of this approach have been demonstrated by the syntheses of other related binary nanoparticular antimonides.[40]

With regard to potential applications of these compounds based on their electronic structure and their semiconducting behavior, the presence of impurities is of utmost importance to understand and judge the performance of the materials. While organic components, such as long chain solvents and surfactants, can be removed by ligand exchange reactions,[41−43] possible impurities and residues from the reactants themselves might not be removed that easily. An important part of addressing these issues is identification of the present compounds, their role during the reaction process, and their presence in the final product.

In this contribution we present a wet chemistry route toward nanoparticular $FeSb_2$ starting from antimony nanoparticles and a molecular iron precursor. Furthermore, we show a 2-fold study of the reaction process: X-ray diffraction allows identification of crystalline phases at intermediate stages of the reaction, while iron-57 Mössbauer spectroscopy elucidates the remaining Fe-containing species during the formation process and determines the purity of the final $FeSb_2$ nanoparticles.

RESULTS AND DISCUSSION

For the $FeSb_2$ synthesis, Sb nanoparticles were dispersed in tetraethylenglycol and then heated at a rate of 15 °C/min under an inert Ar atmosphere. At ~100 °C a dispersion of the Fe precursor (cyclopentadienyl iron(II) dicarbonyl dimer) in tetraethylenglycol was added, and the mixture was heated to 300−310 °C at a rate of 10 °C/min. Reaction intermediates were taken from solution at 200, 250, and 300 °C and after 60 min at that temperature. The products were collected by centrifugation, washed with ethanol, and subsequently dried in an Ar flow.

X-ray Diffraction. X-ray powder diffraction patterns of the reaction intermediates and the final product (Figure 1) reveal that the crystalline $FeSb_2$ phase forms in the temperature interval between 200 and 250 °C. After decomposition of the iron precursor,[44] diffusion of Fe into Sb seems to be the rate-limiting step of the reaction at lower temperatures. At reaction temperatures

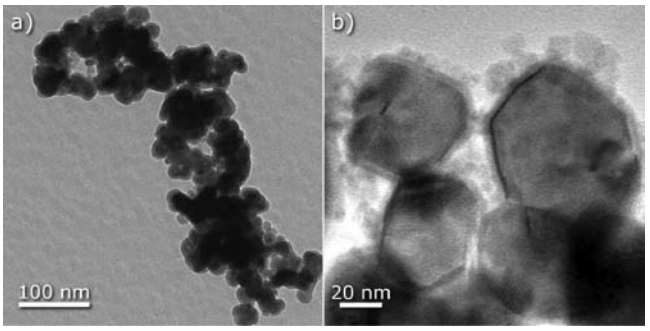

Figure 2. (a) Overview TEM images of the final $FeSb_2$ product consisting of 20−60 nm agglomerates of nanoparticles. (b) TEM image showing $FeSb_2$ particles surrounded by smaller iron oxide particles.

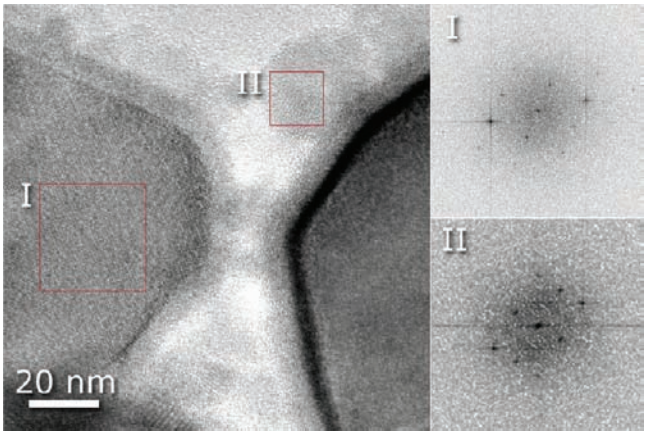

Figure 3. HRTEM image and FFTs of the larger $FeSb_2$ particles (I) and one Fe_3O_4 particle (II).

of 300 °C $FeSb_2$ was the only crystalline phase observed. Even after prolongated heat treatment, no decomposition products were detected.

According to a quantitative phase analysis by Rietveld refinement[17,45] the samples prepared at 200, 250, and 300 °C contain pure Sb, a mixture of approximately 20% Sb and 80% $FeSb_2$, and virtually pure $FeSb_2$, respectively. These values correspond to the *crystalline* components of the intermediate samples at the respective stage of the reaction. The refined lattice parameters of the final product are in good agreement with values reported before (a = 5.8333(5) Å, b = 6.5389(6) Å, and c = 3.2042(3) Å, cf. ref 46). The average crystallite sizes as determined from full pattern refinement are approximately 39(1) nm (cf. Table SI-1, Supporting Information).

TEM Overview. Overview TEM images of the final product (Figure 2) obtained after heating the reaction mixture at ~300 °C for 30 min show porous agglomerates of particles with particle sizes of ca. 20−60 nm. They are in good agreement with the average particle size of about 40 nm, which was determined from refinement of the X-ray diffraction data. Despite intensive sonication during TEM sample preparation, individual particles were never observed, and even the smallest aggregates consisted of several particles.

High-resolution TEM images reveal the presence of smaller particles covering the rim of larger particles (Figure 3). According to the d values determined from the fast Fourier transform

dx.doi.org/10.1021/ic201940r |*Inorg. Chem.* 2011, 50, 11807–11812

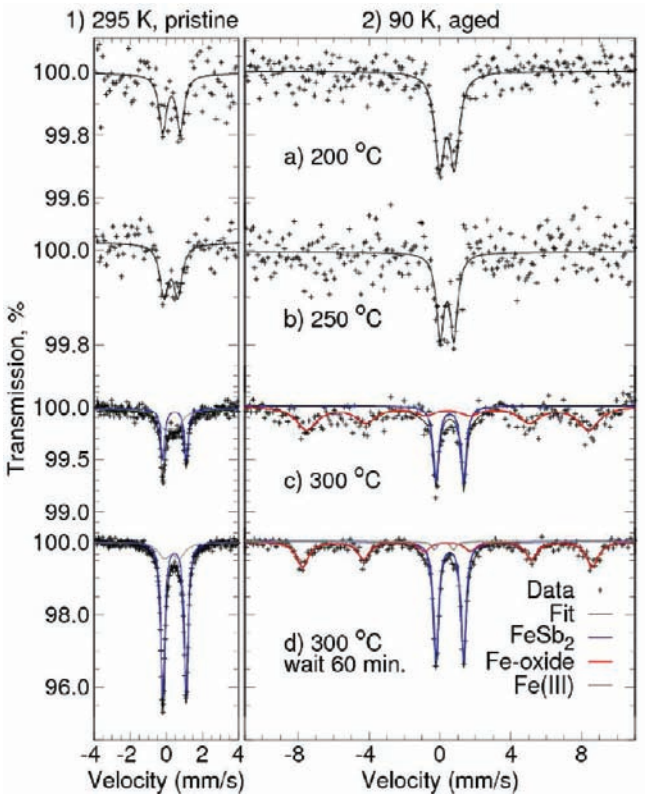

Figure 4. Iron-57 Mössbauer spectra of reaction intermediates measured at 295 K in the pristine state, left, and at 90 K, taken at (a) 200, (b) 250, (c) 300, and (d) 300 °C after 60 min.

(FFT) of the HR-TEM micrographs, the larger particles consist of a $FeSb_2$ core and a comparably thin shell of Fe_3O_4. Due to the low crystallinity and corresponding weak scattering, these impurities are not found in powder X-ray diffraction experiments. However, the Fe_3O_4 shell can easily be removed by treatment with 1 M HCl, and the resulting product is virtually free of magnetic impurities (see Figures SI-1 and SI-2, Supporting Information).

Iron-57 Mössbauer Spectroscopy of Intermediate and Final Products. Iron-57 Mössbauer spectra were measured at 90 and 295 K for a batch of reaction intermediates that were trapped from the reaction vessel at different temperatures (Figure 4) and at five temperatures between 90 and 295 K for the final product of a second batch (Figure 5). Note that the data in Figure 4 were collected from small and varying amounts of samples of about 10−50 mg, which does not allow a quantitative comparison of the iron content for the different spectra. Owing to the small iron amount, the statistics for samples a and b is limited even after long data acquisition (>1 week).

The onset of $FeSb_2$ formation according to the 295 K iron-57 Mössbauer spectra is around 300 °C, and after a subsequent reaction time of 60 min 78% of the iron is transformed to $FeSb_2$ (Figure 4(1) and Table 1). These spectra were collected about 1 or 2 weeks after the synthesis of the samples that were stored in ambient conditions. A second series of spectra of the same samples, again stored under ambient conditions, was measured 3 months later at 90 K, see Figure 4(2), in order to acquire more information about possible superparamagnetic particle impurities. Within statistical error, the spectra of a and b are equivalent and the 90 K measurements reveal that this sample has not

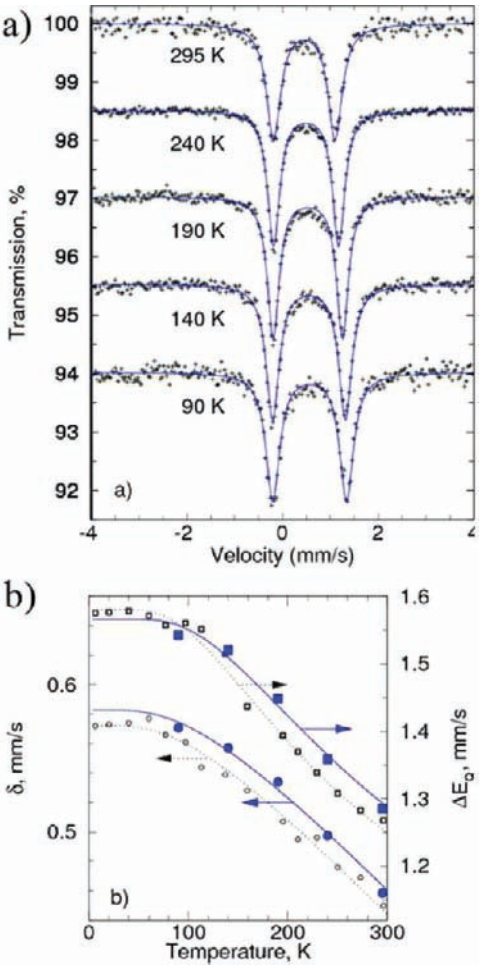

Figure 5. a) Temperature-dependent Fe−Mössbauer data and (b) isomer shift (circles) and quadrupole splitting (squares) of $FeSb_2$ nanoparticles (full symbols) and of bulk $FeSb_2$ (open symbols).[24].

decomposed and there is no evidence for possible superparamagnetic iron or iron oxide. Except for a somewhat larger quadrupole splitting, ΔE_Q, for the pristine sample a, which has only marginal statistical significance, all spectra for samples a and b are indicative of a similar Fe(III) compound that could not been identified. A comparison with literature data showed that this compound has hyperfine parameters very different from the $(CpFe(CO)_2)_2$ precursor, for which the quadrupole splitting of ~1.9 mm/s[47] was reported. This unidentified species could be the intermediate compound with the empirical formula $FeC_2H_2O_6$ identified by Allan[48] for which no Mössbauer spectra seem to be available. The hyperfine parameters are very close to those obtained by Caric et al.[49] for the decomposition product of $FeC_2O_4 \cdot 2H_2O$ after heating at 435 K ($\delta(\alpha\text{-Fe})$ = 0.41(3) and ΔE_Q = 0.82(3) mm/s at 80 K, respectively). The apparent iron content in the samples of the preliminary stages of the reaction, samples a and b, is surprisingly low, which might be due to the iron being weakly bound, i.e., having a low recoil free fraction, in this Fe(III) decomposition product. By comparing the spectral area of the data at 295 and 90 K, i.e., from the temperature dependence of the Lamb−Mössbauer factor, we can estimate the Debye temperature to be 190(50) and 260(50) K for samples a and b.

dx.doi.org/10.1021/ic201940r |Inorg. Chem. 2011, 50, 11807–11812

Table 1. Mössbauer Spectral Parameters Obtained from the Data in Figures 4 and 5

sample	T (K)	$\delta^{\alpha\text{-Fe}}$ (mm/s)	ΔE_Q (mm/s)	percentage	phase	Γ (mm/s)	H^{hf} (T)
$FeSb_2$	295	0.458(5)	1.286(5)	100	$FeSb_2$	0.36(1)	
	240	0.497(5)	1.359(5)	100	$FeSb_2$	0.31(1)	
	190	0.534(5)	1.448(5)	100	$FeSb_2$	0.30(1)	
	140	0.557(5)	1.520(5)	100	$FeSb_2$	0.33(1)	
	90	0.571(5)	1.542(5)	100	$FeSb_2$	0.35(1)	
pristine A	295	0.29(3)	0.98(5)	100	Fe(III)	0.49(8)	
pristine B	295	0.25(5)	0.76(8)	100	Fe(III)	0.56(9)	
pristine C	295	0.458(5)	1.29(1)	48(1)	$FeSb_2$	0.25(1)	
pristine C	295	0.22(5)	0.66(1)	52(4)	Fe(III)	0.86(9)	
pristine D	295	0.455(2)	1.286(2)	78(2)	$FeSb_2$	0.25(1)	
pristine D	295	0.30(5)	0.84(1)	22(2)	Fe(III)	0.78(6)	
aged A	90	0.40(2)	0.84(4)	100	Fe(III)	0.64(6)	
aged B	90	0.40(3)	0.77(5)	100	Fe(III)	0.51(8)	
aged C	90	0.564(6)	1.56(1)	29(1)	$FeSb_2$	0.38(1)	
aged C	90	0.45(3)	0	71(1)	Fe−Ox	1.44(8)	49.4(2)
aged D	90	0.561(7)	1.548(4)	48(1)	$FeSb_2$	0.34(1)	
aged D	90	0.43(1)	0	49(1)	Fe−Ox	0.72(2)	50.7(1)
aged D	90	0.22(3)	1.08(6)	3(1)	Fe(III)	0.34	

The spectra for c and d shown in Figure 4(2) reveal the presence of a large amount of iron oxide with hyperfine parameters similar to those of maghemite nanoparticles.[50,51] The iron(III) impurity seen in the spectra of pristine c and d, Figure 4(1), are thus likely to contain superparamagnetic iron oxide particles. In contrast to sample c, for sample d the amount of iron(III) impurity (in Figure 4(1d)) is much smaller than the amount of iron(III) oxide in Figure 4(2d), and a small amount of another nonspecific iron(III) compound is retained at 90 K. The scenario extracted from these spectra is thus that the dwell time of 60 min promotes progressive formation of $FeSb_2$ but that over a longer period of time only part of this compound is stable against oxidation, whereas for compound c oxidation was likely much faster and the $FeSb_2$ content did not change with time, most likely because of formation of a passivating oxide layer.

The results of the Mössbauer spectroscopic investigations seem at variance with the formation scenario of the crystalline phases deduced from the X-ray diffraction data. As mentioned before the statistics of samples a and b are limited and a reliable statement about the amount of $FeSb_2$ is not possible due to the signal-to-noise ratio. This discrepancy between X-ray diffraction and iron-57 Mössbauer spectroscopy is not unusual as both methods are sensitive to different characteristics.[52] The X-ray diffraction data indicate an onset of the reaction at 250 °C, whereas the Mössbauer spectra do not reveal a measurable amount of $FeSb_2$ for sample b. Because the amorphous content is not observed by XRD, the phase fractions obtained by the Rietveld fits in Figure 1 correspond only to the crystalline fraction, and it is possible that the majority of the iron in sample b is still in molecular or amorphous form, i.e., that the observed 78% of the crystalline fraction correspond to less than the detectable amount of $FeSb_2$ in the Mössbauer spectra of compound b, which we did estimate to be ∼10% from a fit where we constrained the presence of this phase.

The temperature-dependent Mössbauer spectroscopic data in Figure 5a for the second batch of the final product were fitted with a doublet corresponding to $FeSb_2$, and if any, the amount of iron impurities is lower than 5%. The temperature-dependent isomer shift and quadrupole splitting of the $FeSb_2$ nanoparticles are shown in Figure 5b. They are in excellent agreement with the results of Steger and Kostiner for the bulk material.[53,54] The temperature dependence of the isomer shift was fitted with the Debye model for the second-order Doppler shift (Herber, 1984) for our data and that of Steger and Kostiner and yield similar Lamb−Mössbauer temperatures of 430(50) and 400(20) K, respectively, as indicated by the solid and dashed line fit to the isomer shift data in Figure 5b.

The temperature variation of the quadrupole splitting was shown to be related to thermally activated electron delocalization and the magnitude of the gap in bulk $FeSb_2$ is 380 K.[54,56,57] Doping of the compound, e.g., with 25% Co can modify this gap significantly to 480 K.[54] The fit of the data for nano-$FeSb_2$ with the model from ref 55 yields a gap of 460(80) K (Figure 5b). This larger gap could be related either to a modified electronic band structure in the nanoparticles or to a nonideal stoichiometry.

■ CONCLUSION

A solution-based synthesis of $FeSb_2$ nanoparticles was presented, starting from antimony nanoparticles and a molecular iron precursor. This solution synthesis allowed taking "snap shots" of reaction intermediates by evaluating time-dependent X-ray diffraction data. The XRD data revealed the incipient formation of (marcasite-type) $FeSb_2$ between 200 and 250 °C. TEM micrographs exhibit small particles of about 20−60 nm in size covered by a thin "shell"' of iron oxide, as indicated by HRTEM studies. The iron oxide could be removed by HCl treatment as shown by SQUID measurements of an as-prepared and a washed sample. The samples are subject to partial degradation under ambient conditions.

To provide a more detailed insight into the formation process and the final product, iron-57 Mössbauer spectral measurements were conducted on reaction intermediates as well as on the final $FeSb_2$ nanoparticles. The Mössbauer spectroscopic data of the reaction intermediates show an increasing $FeSb_2$ content in the

samples with increasing reaction temperature and time. Samples taken at 200 and 250 °C showed either no or only small amounts of $FeSb_2$, respectively. Together with the results of the X-ray diffraction study, these data show the presence of crystalline antimony and, most likely, molecular iron species at temperatures of around ~200−250 °C which react to form the final $FeSb_2$ nanoparticles.

Due to its sensitivity to all iron-containing compounds including possible amorphous phases not detectable by XRD, the Mössbauer spectroscopic data not only contribute to an understanding of the formation of the $FeSb_2$ nanoparticles but also provide further proof of the quality of the prepared sample.

EXPERIMENTAL SECTION

Synthesis. Tetrahydrofuran was dried with $CaCl_2$ and Na/K and freshly distilled before use. Lithium triethylboronhydride $Li[Et_3BH]$ (Aldrich, 1 M in THF) and $SbCl_3$ (ABCR) were used as obtained; $SbCl_3$ was stored in a glovebox. Trioctylamine (Aldrich) was degassed and stored under Ar before use.

Sb particles were produced by reducing $SbCl_3$ with 3 equiv of the 1 M $Li[Et_3BH]$ solution at room temperature. The black particles were repeatedly redispersed in THF and decanted from solution, dried in vacuum, and kept in a glovebox.

In a typical synthesis, nanoparticles of the nominal composition $FeSb_2$ were prepared by reacting Sb nanoparticles (1 mmol) in tetraethyleneglycol with a heating rate of ~15 °C/min. A dispersion of cyclopentadienyl iron(II) dicarbonyl dimer (0.5 mmol) in approximately 3 mL of tetraethyleneglycol was added to the reaction when the Sb solution reached a temperature of around 100 °C. The reaction mixture was then heated to 300−310 °C at a rate of 10 °C/min and held at that temperature for 60 min. For intermediate products, 2 mL of the solution was extracted by a syringe at approximately 200, 250, and 300 °C and after 60 min.

After cooling to room temperature, the resulting black product was collected by centrifugation (9000 rpm), washed with ethanol, and dried under a steady Ar flow.

X-ray Powder Diffraction. X-ray powder diffraction data were collected with a Bruker-AXS D8-Discover diffractometer in reflection geometry equipped with a HiStar detector using graphite monochromatized Cu Kα radiation. Samples were glued on top of glass and (111) silicon substrates, respectively, using VP/VA copolymer (vinylpyrrolidone/vinylacetate). Le Bail fits and Rietveld refinements were performed with TOPAS Academic v4.1[58] applying the fundamental parameter approach.

Transmission Electron Microscopy. For TEM investigations the sample was suspended in ethanol and dropped onto a carbon-coated copper grid. The images were obtained using a Philips EM420 instrument with an acceleration voltage of 120 kV.

For HRTEM investigations the sample was also suspended in ethanol and sprayed onto a carbon-coated copper grid using the sonifier described in ref 59. The TEM work was carried out with a Tecnai F30 S-TWIN transmission electron microscope equipped with a field emission gun working at 300 kV. High-resolution (HR) TEM and electron diffraction patterns were acquired with a CCD camera (14-bit GATAN 794MSC).

Mössbauer Spectroscopy. Approximately 10 mg of the powder sample was mixed with boron nitride in order to obtain a homogeneous absorber. The iron-57 Mössbauer spectra, at temperatures ranging from 90 to 295 K, were measured on a constant-acceleration spectrometer that utilized a rhodium matrix cobalt-57 source. The instrument was calibrated at 295 K with alpha-iron powder. The sample temperature in the Janis SV-300 cryostat was controlled with a Lake-Shore 330 temperature controller and a silicon diode mounted on the copper sample holder. The accuracy of the sample temperature is better than ±1%.

ASSOCIATED CONTENT

Supporting Information. Refined lattice parameters for the obtained phases and corresponding literature values (Table 1), field cooled and zero field cooled magnetic behavior of a pristine and a cleaned $FeSb_2$ sample (MPMS, Quantum Design; Figure 1), and hysteresis loops at 5 and 300 K of a pristine and a cleaned $FeSb_2$ sample. This material is available free of charge via the Internet at http://pubs.acs.org.

AUTHOR INFORMATION

Corresponding Author

*Phone: +49 6131 392-5135 (W.T.); +49 2461 61-4786 (R.P.H.). Fax: +49 6131 392-5605 (W.T.); +49 2461 61-2610 (R.P.H.). E-mail: tremel@uni-mainz.de (W.T.); r.hermann@fz-juelich.de (R.P.H.).

ACKNOWLEDGMENT

The DFG priority program SPP1386 "Nanostructured Thermoelectrics" is acknowledged for support of this study. C.S.B. and G.K. are recipients of a fellowship from MATCOR, the Graduate School of Excellence of the State of Rhineland-Palatinate. G.K. is a recipient of a fellowship from the Konrad Adenauer Stiftung. R. H. acknowledges support for the Helmholtz-University Young Investigator Group "Lattices Dynamics in Emerging Functional Materials".

REFERENCES

(1) Cable, R. E.; Schaak, R. E. *Chem. Mater.* **2005**, *17*, 6835–6841.
(2) Alivisatos, A. P. *Science* **1996**, *271*, 933–937.
(3) Xie, J.; Zhao, X. B.; Yu, H. M.; Qi, H.; Cao, G. S.; Tu, J. P. *J. Alloys Compd.* **2007**, *441*, 231–235.
(4) Wang, M.i; Zhao, H.; He, J.; Wang, R.; Chen, J.; Chen, N. *J. Alloys Compd.* **2009**, *484*, 864–869.
(5) Matthias, B. T. *Phys. Rev.* **1953**, *92*, 874–876.
(6) Matthias, B. T.; Compton, V. B.; Corenzwit, E. *J. Phys. Chem. Sol.* **1961**, *19*, 130–133.
(7) Matthias, B. T.; Geballe, T. H.; Compton, V. B. *Rev. Mod. Phys.* **1963**, *35*, 1–22.
(8) Bukowski, Z.; Badurski, D.; Stepien-Damm, J.; Troc, R. *Solid State Commun.* **2002**, *123*, 283–286.
(9) McGuire, M. A.; Reynolds, T. K.; DiSalvo, F. J. *J. Alloys Compd.* **2006**, *425*, 81–87.
(10) Meng, J. F.; Polvani, D. A.; Jones, C. D.W.; DiSalvo, F. J.; Fei, Y.; Badding, J. V. *Chem. Mater.* **2000**, *12*, 197–201.
(11) Jones, C. D.W.; Regan, K. A.; DiSalvo, F. J. *Phys. Rev. B* **1999**, *60*, 5282–5286.
(12) Brown, S. R.; Kauzlarich, S. M.; Gascoin, F.; Snyder, G. J. *Chem. Mater.* **2006**, *18*, 1873–1877.
(13) Cox, C. A.; Brown, S. R.; Snyder, G. J.; Kauzlarich, S. M. *J. Electron. Mater.* **2010**, *39*, 1373–1375.
(14) Rauscher, J. F.; Cox, C. A.; Yi, T.; Beavers, C. M.; Klavins, P.; Toberer, E. S.; Snyder, G. J.; Kauzlarich, S. M. *Dalton Trans.* **2010**, *39*, 1055–1062.
(15) Kleinke, H. *Chem. Mater.* **2010**, *22*, 604–611.
(16) Bentien, A.; Johnsen, S.; Madsen, G. K. H.; Iversen, B. B.; Steglich, F. *Eur. Phys. Lett.* **2007**, *80*, 17008/1–17008/5.
(17) Holseth, H.; Kjekshus, A. *Acta Chem. Scand.* **1969**, *23*, 3043–3050.

(18) Hu, R. W.; Mitrovic, V. F.; Petrovic, C. *Appl. Phys. Lett.* **2008**, *92*, 064510.
(19) Hicks, L. D.; Dresselhaus, M. S. *Phys. Rev. B* **1993**, *47*, 12727–12731.
(20) Hicks, L. D.; Dresselhaus, M. S. *Phys. Rev. B* **1993**, *47*, 16631–16634.
(21) Poudeu, P. F. R.; D'Angelo, J.; Downey, A. D.; Short, J. L.; Hogan, T. P.; Kanatzidis, M. G. *Angew. Chem., Int. Ed.* **2006**, *45*, 3835–3839.
(22) Sootsman, J. R.; Kong, H.; Uher, C.; D'Angelo, J. J.; Wu, C.-I; Hogan, T. P.; Caillat, T.; Kanatzidis, M.G. *Angew. Chem., Int. Ed.* **2008**, *47*, 8618–8622.
(23) Karkamkar, A. J.; Kanatzidis, M. G. *J. Am. Chem. Soc.* **2006**, *128*, 6002–6003.
(24) Androulakis, J.; Lin, C. H.; Kong, H. J.; Uher, C.; Wu, C. I.; Hogan, T.; Cook, B. A.; Caillat, T.; Paraskevopoulos, K. M.; Kanatzidis, M. G. *J. Am. Chem. Soc.* **2007**, *129*, 9780–9788.
(25) Vineis, C. J.; Shakouri, A.; Majumdar, A.; Kanatzidis, M. G. *Adv. Mater.* **2010**, *22*, 3970–3980.
(26) Xiao, F.; Hangarter, C.; Yoo, B.; Rheem, Y.; Lee, K. -H.; Myung, N. V. *Electrochim. Acta* **2008**, *53*, 8103–8117.
(27) Barth, J.; Balke, B.; Fecher, G. H.; Stryhanyuk, H.; Gloskovskii, A.i; Naghavi, S.; Felser, C. *J. Phys. D: Appl. Phys.* **2009**, *42*, 185401.
(28) Zelinska, M.; Assoud, A.l; Kleinke, H. *J. Solid State Chem.* **2011**, *184*, 516–522.
(29) Zaikina, J. V.; Jo, Y.-J.; Latturner, S. E. *Inorg. Chem.* **2010**, *49*, 2773–2781.
(30) Whalen, J. B.; Zaikina, J. V.; Achey, R.; Stillwell, R.; Zhou, H.; Wiebe, C. R.; Latturner, S. E. *Chem. Mater.* **2010**, *22*, 1846–1853.
(31) Latturner, S. E.; Stojanovic, M. *J. Solid State Chem.* **2007**, *180*, 907–914.
(32) Leonard, B. M.; Bhuvanesh, N. S. P.; Schaak, R. E. *J. Am. Chem. Soc.* **2005**, *127*, 7326–7327.
(33) Schaak, R. E. *Abstr. Pap., Am. Chem. Soc.* **2005**, *229*, U965–U965.
(34) Cushing, B. L.; Kolesnichenko, V. L.; O'Connor, C. J. *Chem. Rev.* **2004**, *104*, 3893–3946.
(35) Birkel, C. S.; Mugnaioli, E.; Gorelik, T.; Kolb, U.; Panthoefer, M.; Tremel, W. *J. Am. Chem. Soc.* **2010**, *132*, 9881–9889.
(36) Fransson, L. M.L.; Vaughey, J. T.; Benedek, R.; Edstrom, K.; Thomas, J. O.; Thackeray, M. M. *Electrochem. Commun.* **2001**, *3*, 317–323.
(37) Xie, J.; Zhao, X. B.; Cao, G. S.; Zhao, M. J.; Zhong, Y. D. *J. Mater. Sci. Technol.* **2004**, *20*, 344–346.
(38) Bottger, P. H. M.; Valset, K.; Deledda, S.; Finstad, T. G. *J. Electron. Mater.* **2010**, *39*, 1583–1588.
(39) Schlecht, S.; Erk, C.; Yosef, M. *Inorg. Chem.* **2006**, *45*, 1693–1697.
(40) Kieslich, G.; Birkel, C. S.; Stewart, A.; Kolb, U.; Tremel, W. *Inorg. Chem.* **2011**, DOI: 10.1021/ic200074z.
(41) Riha, S. C.; Fredrick, S. J.; Sambur, J. B.; Liu, Y.; Prieto, A. L.; Parkinson, B. A. *ACS Appl. Mater. Interfaces* **2011**, *3*, 58–66.
(42) Kovalenko, M. V.; Spokoyny, B.; Lee, J.-S.; Scheele, M.; Weber, A.; Perera, S.; Landry, D.; Talapin, D. V. *J. Am. Chem. Soc.* **2010**, *132*, 6686–6695.
(43) Kovalenko, M. V.; Scheele, M.; Talapin, D. V. *Science* **2009**, *324*, 1417–1420.
(44) Nakhjavan, B.; Tahir, M. N.; Gao, H.; Schladt, T.; Schneider, K.; Natalio, F.; Ament, I.; Branscheid, R.; Weber, S.; Schröder, H. C.; Müller, W. E. G.; Kolb, U.; Sönnichsen, C.; Schreiber, L. M.; Tremel, W. *J. Mater. Chem.* **2011**, *21*, 8605–8611.
(45) Trzebiatowski, W.; Bryjak, E. *Z. Anorg. Allg. Chem.* **1938**, *238*, 255–267.
(46) Melnyk, G.; Tremel, W. *J. Alloys Compd.* **2003**, *349*, 164–171.
(47) Herber, R. H. *Hyperfine Interact.* **1997**, *108*, 549–561.
(48) Allan, J. R.; Paton, A. D. *Thermochim. Acta* **1994**, *231*, 333–335.
(49) Caric, S.; Marinkov, L.; Slivka, J. *Phys. Status Solidi A: Appl. Res.* **1975**, *31*, 263–268.
(50) Morup, S.; Bodker, F.; Hendriksen, P. V.; Linderoth, S. *Phys. Rev. B* **1995**, *52*, 287–294.
(51) Rebbouh, L.; Hermann, R. P.; Grandjean, F.; Hyeon, T.; An, K.; Amato, A.; Long, G. J. *Phys. Rev. B* 2007, *76*.
(52) Long, G. J.; Cheetham, A. K.; Battle, P. D. *Inorg. Chem.* **1983**, *22*, 3012–3016.
(53) Steger, J.; Kostiner, E. *J. Solid State Chem.* **1972**, *5*, 131–135.
(54) Hu, R.; Hermann, R. P.; Grandjean, F.; Lee, Y.; Warren, J. B.; Mitrovic, V. F.; Petrovic, C. *Phys. Rev. B* **2007**, *76*, 224422.
(55) Herber, R. H. *Chemical Mössbauer Spectroscopy*; Plenum Press: New York, 1984.
(56) Gerard, A.; Grandjean, F. *J. Phys. Chem. Solids* **1975**, *36*, 1365–1370.
(57) Goodenough, J. B. *J. Solid State Chem.* **1972**, *5*, 144–152.
(58) Coelho, A. *TOPAS Academic V4.1*; Coelho Software: Brisbane, Australia, 2007.
(59) Mugnaioli, E.; Gorelik, T.; Kolb, U. *Ultramicroscopy* **2009**, *109*, 758–765.